analytical chemistry

Article

pubs.acs.org/ac

# Two New Devices for Identifying Electrochemical Reaction Intermediates with Desorption Electrospray Ionization Mass Spectrometry

Heyong Cheng,[†,‡] Xin Yan,[†] and Richard N. Zare*[,†]

[†]Department of Chemistry, Stanford University, Stanford, California 94305-5080, United States

[‡]College of Material Chemistry and Chemical Engineering, Hangzhou Normal University, Hangzhou, 310036, China

Supporting Information

**ABSTRACT:** Desorption electrospray ionization mass spectrometry (DESI-MS) previously has been used to capture and identify transient intermediates in electrochemical redox reactions on a platinum-covered rotating waterwheel. We present here two different setups that use a flat surface with porous carbon tape as the working electrode, where analyte-containing microdroplets from the DESI probe contacted with electrolyte supplied onto the surface. One setup had the conducting carbon tape in the form of a grooved inclined plane; the other one was in the form of a flat plane that had the conducting carbon tape as its front surface. Both these setups, which were relatively robust and easy to operate, overcame interference from the electrospray sheath gas that disturbs and dries the flowing electrolyte. By using the inclined-plane device, we observed radical cations and dimer species generated in the electrochemical oxidation of triphenylamine, diimine and imine alcohol in the electrochemical oxidation of uric acid, and the reductive cleavage of disulfide bonds in glutathione disulfide. By using the device with the flat carbon tape, we detected nitrenium ions generated in the electrochemical oxidation of *N*,*N*′-dimethyoxydiphenylamine and di-*p*-tolylamine. Our experience suggests that the flat porous carbon tape surface might be preferable over the inclined plane because of its ease of setup.

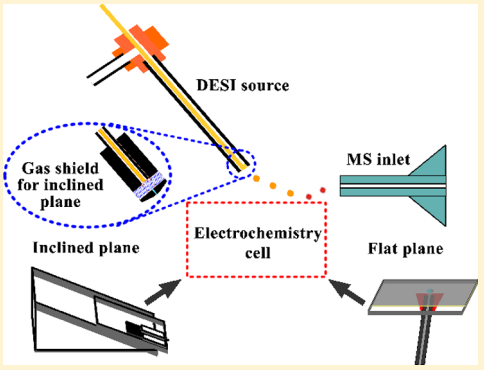


Identifying and monitoring transient intermediates produced in electrochemical reactions are essential for mechanistic studies of redox reactions, including many biological redox processes.[1,2] Traditional methods used for these studies involve cyclic voltammetry,[3] spectroelectrochemistry,[4] and surface scanning probe techniques,[5] which suffer from low chemical specificity and/or low detection capabilities regardless of ultrafast response from microsecond to nanosecond by scanning electrochemical microscopy (a surface scanning probe technique). The versatility of mass spectrometry (MS) for label-free, highly sensitive, selective, and real-time detection of molecular weight and structural discrimination makes its marriage with electrochemistry (EC) appealing.

An effective interface between electrochemistry and mass spectrometry to efficiently introduce electrochemical products into a mass spectrometer is a challenge.[6] As early as 1971, Bruckenstein and Gadde[7] reported the first EC-MS device for *in situ* detection of volatile electrode reaction products by electron impact MS based on a Teflon membrane. Following the pioneering work, various ionization techniques in MS have been widely used for the online coupling of EC-MS over the last 4 decades, which include thermospray (TS),[8−10] fast atom bombardment (FAB),[11] electrospray ionization (ESI),[12−14] desorption electrospray ionization (DESI),[15−18] liquid sample DESI[19−21] and nanoDESI,[22] and differential electrochemical mass spectrometry (DEMS).[23] Considering the short lifetimes of electrochemically generated intermediates, having a rapid response time from electrolysis solution to gas-phase MS detection is vital. DEMS has been shown to have a short response time down to 0.1 s.[23] However, a transferring capillary is commonly used to allow electrolytic solution flowing from electrochemical cells to ionization sources in most EC-MS couplings based on TS, FAB, ESI, liquid sample DESI, and nanoDESI sources. The capillary offers a typical response time of several seconds. Xu et al.[13] presented an in-source interface for EC-ESI-MS with a fast response, where a Pt microcylinder (working electrode) protruded (0−3 mm) from a stainless-steel capillary (auxiliary electrode and ESI emitter). The design greatly reduced the delay time (∼1.7 s) between electrochemical reaction and detection. ESI high voltage interfered with electrochemical reactions, which can be solved either by floating or by decoupling the EC system from ESI source. DESI has been shown to sampling analytes by splashing, which makes EC-DESI coupling simple due to physical separation of DESI probes from EC. Miao and Chen[19] reported a tubular setup for EC-DESI, where the floating or decoupling was eliminated. By taking advantages of the fast sampling time of DESI on the

**Received:** December 26, 2016
**Accepted:** January 27, 2017
**Published:** January 27, 2017





DOI: 10.1021/acs.analchem.6b05124
*Anal. Chem.* 2017, 89, 3191−3198

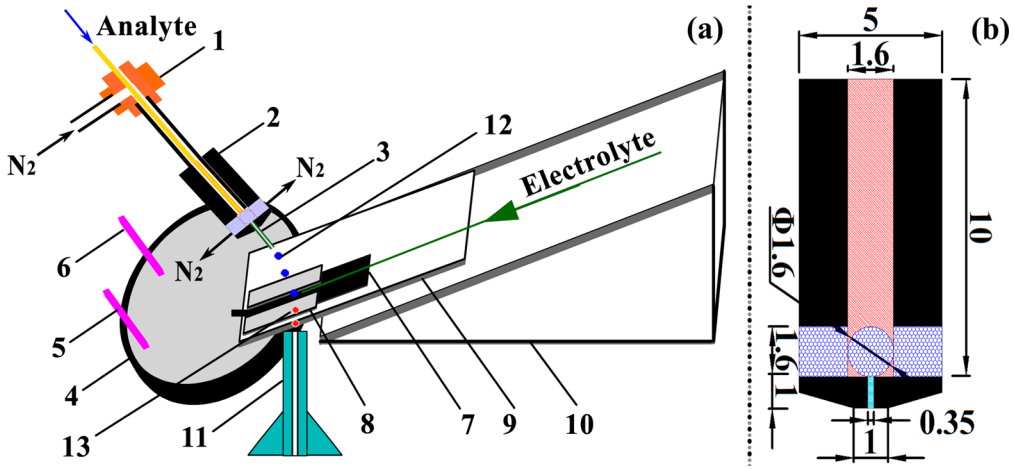


**Figure 1.** EC-DESI on a grooved, inclined plane: (a) schematic diagram and (b) close-up of the gas shield (dimensions given in mm). (1) DESI probe, (2) gas shield, (3) inserted capillary, (4) culture dish with electrolyte, (5) reference electrode, (6) counter electrode, (7) carbon paper (served as working electrode), (8) glass subslide cover, (9) glass slide substrate, (10) 30° triangular platform, (11) MS inlet, (12) primary microdroplets, (13) secondary microdroplets.

order of milliseconds and freedom of floating or decoupling,[24] Brown et al. achieved a delay time on the millisecond scale by developing a rotating waterwheel setup for coupling EC to DESI.[15−17] The working electrode surface was *in situ* sampled by splashing primary microdroplets from a custom spray source for fast transfer of electrogenerated species into the MS inlet. However, the setup requires careful tuning for better performance (mainly the position adjustment of the waterwheel and the DESI sprayer relative to the MS inlet).

The objective of this study is to improve reproducibility, simplify, and strengthen instrumentation for EC-DESI coupling. We describe two new simple setups. Each uses either a grooved inclined carbon tape or a flat-surfaced carbon tape as the working electrode. The carbon tape consists of carbon paper having an adhesive backing.

For the setup with the grooved inclined plane, two modifications were made for the EC-DESI coupling (see Figure 1a). First, the electrolyte solution was flowed on the surface of a piece of carbon paper (working electrode) along a 2 mm channel. The carbon paper held the electrolyte in the presence of $N_2$ of a moderate pressure, offering a wetted surface. Second, primary microdroplets were isolated from the nebulizing $N_2$ by a gas shield. The microdroplets then struck the wetted carbon paper. In such a design, there was no adverse effect from the nebulizing gas pressure and there was no need to optimize the electrolyte flow rate. Electrochemical reactions could occur only if the carbon paper surface was wet. Electro-oxidation of triphenylamine (TPA) and uric acid, and electro-reduction of glutathione disulfide (GSSG) were then performed to demonstrate the feasibility of the first design.

For the EC-DESI coupling based on a flat plane surfaced with carbon tape (see Figure 2), electrolyte solution was flowed from a stainless-steel tube onto the carbon paper surface (which was the working electrode). The carbon paper isolated the electrolyte from high-pressure nebulizing gas but linked the sprayed microdroplets with electrolyte, ensuring reliable measurement of the electrochemical reactions. The design also simplified operation by eliminating instrumentation optimization prior to running an experiment. The feasibility of the second EC-DESI coupling was demonstrated by online monitoring of nitrenium ions in electro-oxidation of 4,4′-dimethyoxydiphenylamine (DMDPA) and di-*p*-tolylamine

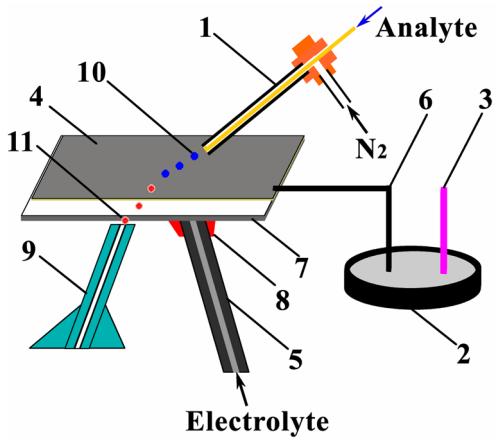


**Figure 2.** Schematic diagram of EC-DESI on a carbon-tape-surfaced flat plane. (1) DESI probe, (2) culture dish with electrolyte, (3) reference electrode, (4) carbon paper (served as working electrode), (5) 1/16 in stainless steel tubing (served as counter electrode), (6) platinum wire connected to carbon paper and electrolyte in culture dish, (7) glass slide cover containing an access hole, (8) PEEK ferrule, (9) MS inlet, (10) primary microdroplets, (11) secondary microdroplets.

(DPTA). The choice of which electrochemical studies to carry out on the two different setups was arbitrary.

## EXPERIMENTAL SECTION

**Chemicals and Reagents.** Throughout an experiment, ultrapure water with a resistivity of 18.2 MΩ cm was prepared from a Milli-Q Plus water purification system (Millipore, Bedford, MA). All of the reagents were of analytical or chromatographic grade and were used without further purification. All solutions were subjected to filtration using 0.22-$\mu$m membrane filters and ultrasonication for 10 min prior to use. Ammonium acetate (97%) and uric acid (99%) were purchased from Sigma-Aldrich. Triphenylamine (99%) was obtained from Acros Organics. Lithium triflate (LiOTf, 96%), 4,4′-dimethyoxydiphenylamine (99%), di-*p*-tolylamine (97%) tetrabutylammonium hexafluorophosphate (98%), and L-glutathione oxidized (98%) were also supplied by Sigma-


DOI: 10.1021/acs.analchem.6b05124
*Anal. Chem.* 2017, 89, 3191−3198

Aldrich. Glacial acetic acid, ammonium hydroxide, and acetonitrile (HPLC grade) were provided by Fisher Scientific.

**Instrumentation.** All MS data were acquired on an LTQ Orbitrap XL hybrid mass spectrometer (Thermo Fisher Scientific, San Jose, CA). The Orbitrap ion transfer capillary was held at 275 °C for all analyses. High voltage was not applied to the sample spray to minimize in-source electrochemistry. The resolution was set to 30 000 at $m/z$ = 400 for triphenylamine and glutathione disulfide experiments and 60 000 at $m/z$ = 400 for other experiments. All data were analyzed using the Qual Browser feature of the Xcalibur program (Thermo Fisher Scientific, San Jose, CA). Analyte solutions were infused through a fused-silica capillary tubing (50 μm i.d., 150 μm o.d.) surrounded by a stainless-steel capillary (190 μm i.d., 1.60 mm o.d.), which directed the 150 psi nebulizing $N_2$ gas, using a custom-built source.

For EC-DESI on a grooved inclined plane, the ESI source was positioned ∼2 mm above the grooved carbon paper and ∼1.6 mm away from the channel. The inlet of the transfer capillary was placed ∼0.5 mm above the carbon paper and almost touching the channel. The inclined plane was held by a 30° triangular platform. For EC-DESI on a flat front-surfaced plane, the source was positioned ∼2 mm above the carbon paper and ∼4 mm away from the MS inlet. The inlet of the transfer capillary was placed ∼0.5 mm below the carbon paper and ∼1 mm far from the glass slide edge.

Pieces of plain carbon paper from AvCarb Material Solutions (Lowell, MA) were pasted on the grooved and the front surface to serve as the working electrode in the two setups. A plain carbon cloth also from AvCarb Material Solutions was used as the counter electrode. Potentials between the two-electrode system were supplied by a dc power supply with an output voltage ranging from 0 to ±500 V (model 313B, Bertan Associates Inc.). Earlier experiments were carried out with the three-electrode system (a working electrode, a counter electrode, and a Ag/AgCl reference electrode from BASi (West LaFayette, IN)), but we removed the standard reference electrode in later experiments since both the two-electrode system and the three-electrode system offered similar results with TPA as the model (see the Supporting Information "Comparison of electrochemical behaviors by the two-electrode and three-electrode system"). In the three-electrode system of the inclined device, the typical current is submilliamperes and the typical resistance between the working electrode and the counter electrode, which are separated by about 5 mm, is kiloohms. In three-electrode system of the flat surfaced device, the typical current is microamperes, and the typical resistance between the working electrode and the counter electrode, which are separated by about 2 mm, is submegaohms. The $iR$ drop for both systems was millivolts. Potentials across the three-electrode system were controlled by a potentiostat (WaveNow, Pine Research Instrumentation, Durham, NC). The flowing electrolyte solution was fed by a model 35-2226 syringe pump (Harvard Apparatus Inc.) with a 10 mL glass syringe.

**Fabrication of Grooved and Flat Front-Surfaced Planes and Gas Shield.** The grooved plane was fabricated in the following procedure: A 15 mm × 15 mm × 0.2 mm glass slide was cut into two cover subslides (2 mm × 15 mm × 0.2 mm and 13 mm × 15 mm × 0.2 m). A 25 mm × 75 mm × 1 mm glass slide substrate was washed with acetonitrile and dried in the air. Then both glass subslides were covered on the surface of the glass substrate with epoxy resin to form a 2 mm-wide channel. Next, a piece of carbon paper was pasted on the channel by epoxy resin to serve as the working electrode.

The flat front-surfaced plane was fabricated in the following procedure: An access hole was first drilled into a 10 mm × 25 mm × 1 mm glass slide with a 0.4 mm-diameter diamond-tipped drill bit at the 2 mm × 12.5 mm site. After washing with ultrapure water and drying completely, the top surface of the glass substrate was then covered with a piece of 8 mm × 25 mm plain carbon paper (AvCarb Material Solutions, Lowell, MA), pasted on with epoxy resin, which served as the working electrode. Next, a PEEK ferrule was fixed by epoxy resin on the bottom surface of the substrate covering the hole. Finally, a 5 cm stainless-steel tubing (0.02 in. i.d. and 1/16 in. o.d.) as the counter electrode was inserted into the PEEK ferrule with the joint sealed by epoxy resin.

A schematic diagram of gas shield is shown in Figure 1b. The gas shield was machined from PEEK material. The red horizontal hole of 1.6 mm in diameter and 10 mm in length was for the custom spray source whereas the cyan horizontal hole of 0.35 mm in diameter and 1 mm in length served as a passage way for microdroplets. The other four cross holes of 1.6 mm in diameter and 1.7 mm in length were pathways for nebulizing $N_2$ gas. A 2 mm fused-silica capillary of 350 μm o.d. and various inner diameters was inserted into the cyan horizontal hole to further decrease the bore diameter.

## RESULTS AND DISCUSSION

**EC-DESI on a Grooved Inclined Plane.** The *in situ* probing of the transient intermediates in electrochemical reactions was achieved by DESI-MS with a delay time on the milliseconds order.[15−17] In these studies, electrochemistry took place on the surface of the working electrode when the primary microdroplets from a spray source struck the surface to produce secondary microdroplets by splashing. However, it is necessary to adjust positions of the waterwheel and the DESI sprayer relative to the MS inlet, which is time-consuming. Here, we made the instrumentation and experimental process simple, robust, and reliable with respect to the working electrode and the nebulizing gas.

**Gas Shield Operation.** The high-flow-rate nitrogen gas needed for microdroplet generation could blow the electrolyte solution off the surface of the working electrode and also make it dry, restricting microdroplets from direct contact with the electrolyte and finally leading to electrolysis failure. Although the nitrogen gas flow rate could be dramatically decreased by turning down the gas pressure for the DESI source, it is insufficient to eliminate the above adverse effect from nitrogen gas from the preliminary experiment. What is worse in this case is that the sensitivity was dramatically decreased due to poor spraying of primary microdroplets and low conversion into secondary microdroplets by splashing. A gas shield was therefore introduced to remove the bulk nebulizing gas but to allow microdroplet passage. As shown in Figure 1b, each large-bore cross hole had a sectional area of 2.01 $mm^2$, whereas the single axial small-bore cyan hole had a sectional area of 0.096 $mm^2$. The large difference in sectional area (nearly 84-fold) ensured that nitrogen gas, when it entered the gas shield, primarily flowed out from the four large radical holes and not mostly from the only small axial hole. Furthermore, the small axial hole could be further downscaled to 50−250-μm-diameter by inserting a short fused-silica capillary (50−250 μm i.d. and 350 μm o.d.). The sectional area of the small axial hole thus varied in the range from 0.002 to 0.049 $mm^2$. This variation


DOI: 10.1021/acs.analchem.6b05124
Anal. Chem. 2017, 89, 3191−3198

causes the sectional area ratio of radial holes to axial hole to range from 164 to 4020. Therefore, much less nebulization gas passed through the axial hole under these circumstances. In this manner, most of the nitrogen gas was removed from the microdroplets. However, the sample capillary of the customized spray source was concentric to the axial hole, allowing microdroplets to fly through the axial hole. Besides, the cross four holes were arranged in the radial directions symmetrically, inhibiting the interference on the moving direction of the microdroplets caused by the nitrogen gas. Two simple comparison experiments were performed to test the functions of the gas shield.

The custom sprayers, without and with gas shield of 75-$\mu$m and 350-$\mu$m axial holes, were sprayed toward three culture dishes half-filled with water. A turbulent water vortex was induced by the nebulizing gas without a gas shield (see video in the Supporting Information). However, very weak whirling flows were produced with a gas shield of a 350-$\mu$m axial hole (see video in the Supporting Information). A water whirlpool was not observed from the remaining nebulizing gas with a gas shield with a 75-$\mu$m axial hole (see video in the Supporting Information). These videos have provided strong proof for the removal of nebulizing gas by the gas shield.

Quantitative experiments were carried out to confirm microdroplet passage and determine the passage percentages. TPA was selected as the target for reasons that will be explained later; MS intensities at $m/z$ 246.1277 (the protonated TPA cation) with gas shields of various parameters were recorded. As shown in Figure S1a, the signal ratio (MS intensities with gas shield of various axial bores to that without a gas shied) sharply fell with the decreasing bore diameter. The signal intensity with a gas shield of 75-$\mu$m axial hole was only 1/50th of that without a gas shield. The results indicated that only a few microdroplets could pass the gas shield. A gas shield of the 150-$\mu$m axial hole was selected for the electrochemical application as a compromise between gas removal and microdroplet passage. Figure S1b shows variation of MS intensity by altering the tip-to-bore distance. When the sprayer was moved toward the axial hole (decreasing the distance), the abundance at $m/z$ 246.1277 was dramatically enhanced. It may be ascribed by the sector distribution of microdroplets after nebulization. Fewer microdroplets passed through the axial hole at a longer distance, leading to a lower response. The tip-to-bore distance was selected to be 0.1 mm for best sensitivity. Figure S1c demonstrates the relationship between the signal and the length of the 150-$\mu$m-i.d. capillary inserted into the 0.35 mm axial hole. As the length of the inserted capillary increased, the MS intensity was significantly reduced. The reason may be microdroplets adhering to the inner surface of the long capillary. The inserted capillary length was chosen to be 2 mm for best sensitivity.

**Working Electrode Material.** The material to fabricate the working electrode is important for electrochemical reactions. In the preliminary experiment, we tried a platinum thin layer as the working electrode, which was deposited on the full surface of the glass slide substrate with a depth of 100 nm. The hitting center of the electrolyte liquid film at the platinum layer surface became thinner because of the spray microdroplets along with the remaining nebulizing gas from the gas shield. A visible pore was observed at the hitting center and no signal of electrolytic products was detected by MS detector at low flow rates below 21 $\mu$L min$^{-1}$. However, the MS intensity of the protonated TPA ion was found to be significantly reduced without any signal of oxidation products at high flow rates above 37 $\mu$L min$^{-1}$. We could only occasionally observe the radical TPA cation at a very low level at electrolyte flow rates around 29 $\mu$L min$^{-1}$. The observations indicated that the conditions to obtain a suitable deep liquid film were difficult to control. This problem was solved by introducing a gas shield and carbon paper as the working electrode, which ensured that the new setup was easily tuned and not sensitive to the positions of surface and the DESI sprayer relative to the MS inlet in comparison with the waterwheel design.[15−17] Besides, we also observed the breakdown of the platinum layer due to electrodissolution after a certain time (>2 h) with high potentials (>4 V).

We turned to a piece of thin carbon paper (approximately 0.25 mm) which had a good air permeability (15 s/100 cc) and an excellent through-plane sensitivity (7.8 mOhm cm$^2$). In comparison with the deposited platinum layer, the carbon paper offered four figures of merit. First, it could be conveniently cut into any shape and then be attached onto a glass slide, eliminating the expensive, time-consuming, and tedious Pt-deposition procedure. Second, it could withstand high potentials during electrolysis (no breakdown at ±100 V for 2 h), offering a long time for the coupling. Third, it could hold electrolyte by its inherent pores even in the presence of bulk nebulizing gas, ensuring direct contact of the electrolyte with the microdroplets. Fourth, its rough insulating surface generates a large surface area, increasing the contact area and reaction time of the microdroplets on the working electrode.

By using the carbon paper as the working electrode, we investigated electrochemical oxidation of TPA at various electrolyte flow rates. As shown in Figure S2a, radical TPA cations and dicationic dimer intermediates were observed at electrolyte flow rates down to 1 $\mu$L min$^{-1}$. The MS intensities for both intermediates grew significantly on increasing the electrolyte flow rates up to 10 $\mu$L min$^{-1}$ and reached a signal plateau with increased flow rate. The relative standard deviations (RSDs, $n$ = 3) for both signals also were gradually improved with the electrolyte flow rate; satisfactory precisions below 6% were obtained at electrolyte flow rates higher than 2 $\mu$L min$^{-1}$. This improvement resulted from the last two advantages of the carbon paper. We also observed that no electrochemical reactions could occur if the carbon paper was dried. It is therefore important to maintain a wetted surface by prewetting the carbon paper before electrochemistry and continuously feeding the electrolyte onto the carbon paper's surface at flow rates above 1 $\mu$L min$^{-1}$. Electrolyte fed at 10 $\mu$L min$^{-1}$ was chosen to give best intensities.

The potential applied on the carbon paper was varied to investigate its effect on signal intensities of electrolytic intermediates by using the two-electrode system. As demonstrated in Figure S2b, the abundances of $m/z$ 245.1195 and 488.2230 were significantly enhanced by increasing the applied potential to 3 V. A slow ascendance was obtained with higher potential up to 5 V. Further increasing potential resulted in stable intensities. Besides, no observable breakdown of the carbon paper was encountered for a long period (up to 2 h) at high potentials (±100 V).

**EC-DESI on a Flat Plane with a Carbon-Tape Surface.** Although the first EC-DESI coupling simplified instrumentation and experimental process as well as improved the reproducibility by using carbon tape grooved inclined plane, the sensitivity was limited by the gas shield. We therefore designed a simpler DESI-MS instrumentation for electro-


DOI: 10.1021/acs.analchem.6b05124
Anal. Chem. 2017, 89, 3191−3198

**Scheme 1. Oxidation Steps and Ion Formation Pathways of Uric Acid**

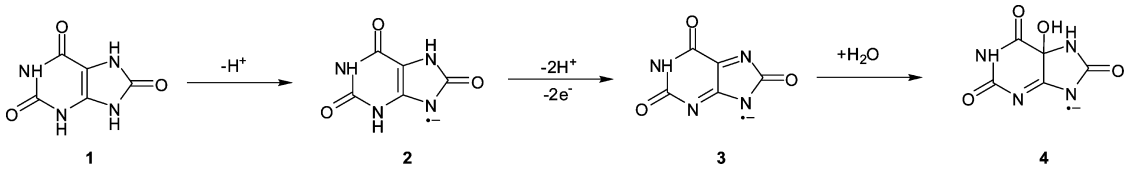


chemical applications using a flat carbon-tape-surfaced plane. In this design, the electrolyte was flowed onto the carbon paper out of the end-column at the bottom tubing to keep a wetted surface. The porous carbon paper was a shield to isolate the electrolyte from the nebulizing gas. It also served as a bridge to link the microdroplets to the electrolyte. The electro-oxidation reactions could occur only if the carbon paper was wetted. MS intensities of TPA and a TPA dimer (*N*,*N*,*N*′,*N*′-tetraphenylbenzidine, TPB) radical cations in the electro-oxidation of TPA were found to be very stable using ammonium acetate at flow rates above 0.5 $\mu$L min$^{-1}$ (Figure S3), proving the independence of electrochemistry from the electrolyte flow rate. In other words, instrumentation optimization prior to experiment was eliminated. However, minimum electrolyte should also be fed to prevent the carbon paper from drying by the nebulization gas. For instance, 0.3 $\mu$L min$^{-1}$ water or 19 $\mu$L min$^{-1}$ acetonitrile is necessary to keep a wetted surface in our experiment. Nevertheless, excessive supply of electrolyte onto the carbon paper may lead to electrolyte accumulation on the surface, which should be removed occasionally by absorbing paper. We found that the flat porous carbon tape surface might be preferable over the grooved incline plane because of its ease in setting it up and low cost whereas the grooved inclined carbon tape plane might be advantageous in electrolyte waste collection.

**Electro-Oxidation of Uric Acid.** Uric acid, which is excreted in urine, is a metabolic product of purine nucleotides by enzymatic oxidation. Its presence in blood and urine is a good indicator for a variety of medical conditions. In consideration of its biologically important roles and well-studied electrochemical oxidation pathways, uric acid was chosen to investigate the feasibility of EC-DESI with the inclined plane. This choice was made after the success we had with TPA electrochemical oxidation (see Supporting Information "Electrochemical oxidation of TPA"). The well-known mechanism for electro-oxidation of uric acid (Scheme 1) initiates with a loss of two electrons and two protons from uric acid (**1**), leading to an unstable diimine product (**3**) and terminates with a further hydration of the diimine species to yield the imine alcohol (**4**).[16]

When spraying 100 $\mu$M uric acid in 1% acetic acid at a flow rate of 5 $\mu$L min$^{-1}$ onto the surface of the wetted carbon paper without applied potential, the deprotonated uric acid anion $[UA - H]^-$ (**2**) was observed at *m*/*z* 167.0209 (theoretical *m*/*z* 167.0211, error −1.2 ppm) (Figure 3a). After applying an oxidation potential of 5 V across the carbon paper, two new peaks at *m*/*z* 165.0052 and 183.0157 were observed (Figure 3a), which corresponded to the diimine intermediate $[UA - 3H]^-$ (**3**) (theoretical *m*/*z* 165.0054, error −1.2 ppm) and the imine alcohol $[UA - 3H + H_2O]^-$ (**4**) (theoretical *m*/*z* 183.0160, error −1.6 ppm), respectively. Upon CID (see the Supporting Information Figure S6), the diimine (**3**) and imine alcohol (**4**) species both lost CONH, leading to the formation of two fragment ions at *m*/*z* 121.9997 (theoretical *m*/*z* 121.9996, error +0.8 ppm) and 140.0102 (theoretical *m*/*z* 140.0102, error 0 ppm), respectively.[10] Enhanced crests and reduced troughs in the profiles were reproducibly observed in the presence and absence of oxidation potential, respectively, as shown in the EICs (Figure 3b) at *m*/*z* 165.0052 (**3**) and 183.0157 (**4**). Clearly, both species originated from the electro-oxidation of uric acid. It is worth noting that this was the first simultaneous MS observation of the unstable diimine and imine alcohol.

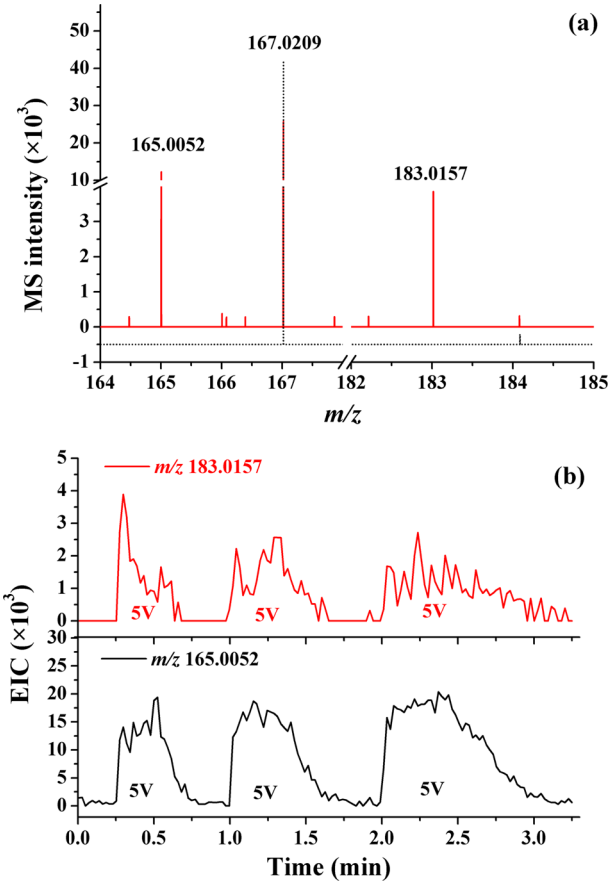


**Figure 3.** (a) Negative-ion-mode mass spectra of uric acid with zero (gray) and 5 V (red) applied to the carbon paper. (b) Ion chronograms showing extracted ion counts for the imine alcohol anion at *m*/*z* 183.0157 (red) and the diimine radical anion at *m*/*z* 165.0052 (black) as the potential is turned on and off.

**Electro-Reduction of GSSG.** Cleavage of disulfide bonds is highly desirable in the structural analyses of peptides and proteins. Compared with the traditional protocol by chemical reduction, electrolytic reduction to break disulfide bond is free of reduction reagents and byproducts. Glutathione disulfide is a simple cysteine-containing tripeptide derived from two glutathione (GSH) molecules, which are important antioxidants in plants, animals, and some bacteria.

We tested GSSG for disulfide breakdown by electro-reduction using EC-DESI-MS on an inclined plane. We



DOI: 10.1021/acs.analchem.6b05124
*Anal. Chem.* 2017, 89, 3191−3198

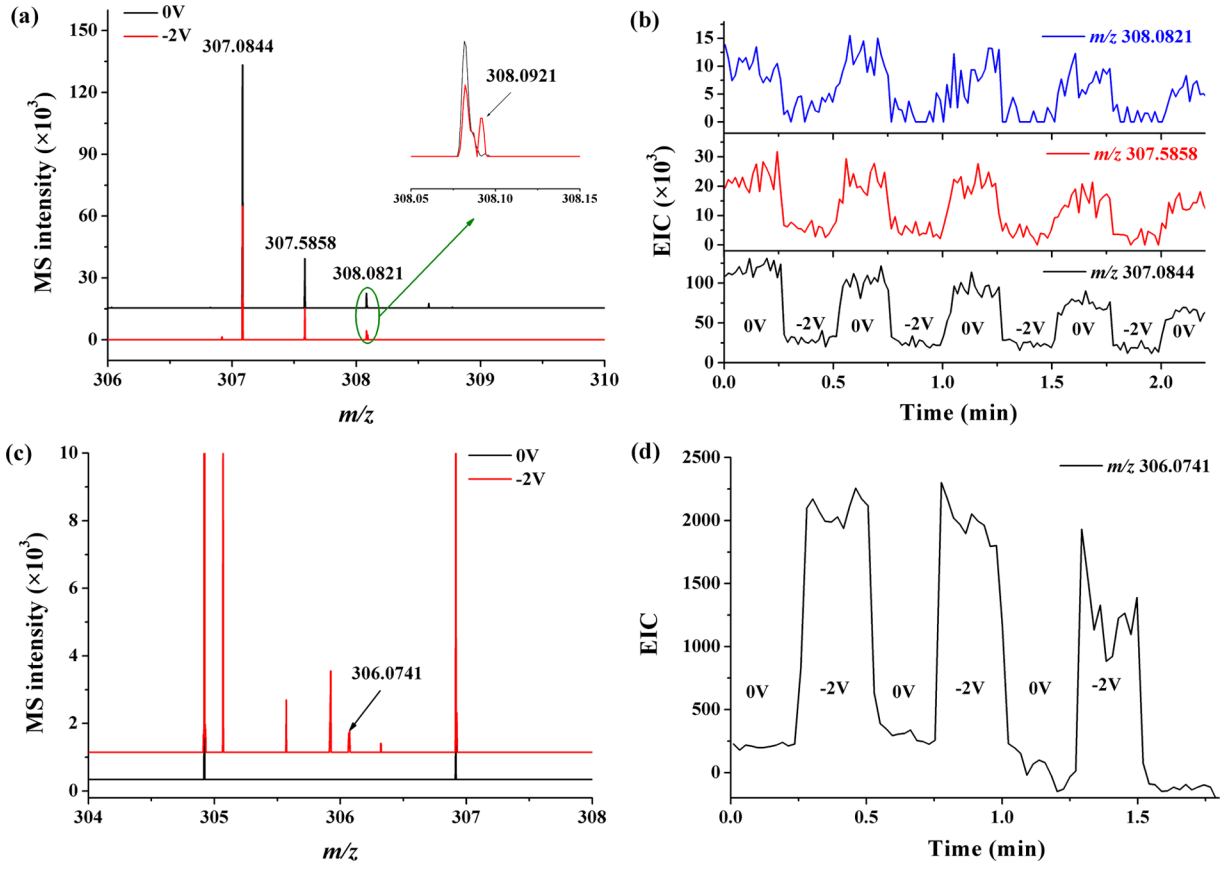


**Figure 4.** Mass spectra of GSSG with zero (black) and −2 V (red) applied to the carbon paper: (a) positive-ion-mode and (c) negative-ion-mode. (b) Ion chronograms under positive-ion-mode showing extracted ion counts for GSSG containing $^{34}S$ at $m/z$ 308.0821 (blue) $^{13}C$ at $m/z$ 307.5858 (red) and normal GSSG at $m/z$ 307.0844 (black) as the potential is turned on and off. (d) Ion chronograms under negative-ion-mode showing extracted ion counts for GSH at $m/z$ 306.0741 (black) as the potential is turned on and off.

**Scheme 2. Oxidation Steps and Ion Formation Pathways of DMDPA**

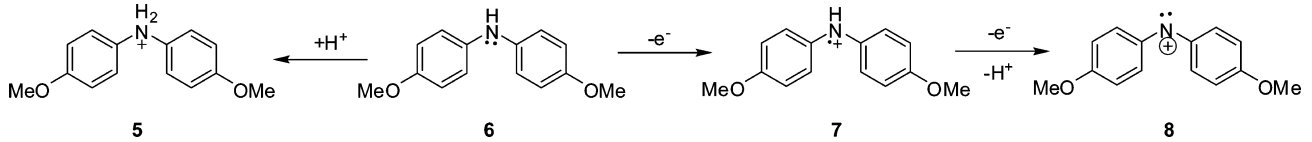


collected mass spectra in the positive mode when microdroplets of 100 μM GSSG in 1% acetic acid were splashed at the surface of the wetted carbon paper with zero potential. The doubly charged dication $[GSSG + 2H]^{2+}$ appeared in the mass spectrum in Figure 4a at $m/z$ 307.0844 (theoretical $m/z$ 307.0838, error +2.0 ppm). Along with the dication, we also observed its two major isotope peaks at $m/z$ 307.5858 (theoretical $m/z$ 307.5855, error +1.0 ppm) and 308.0821 (theoretical $m/z$ 308.0817, error +1.3 ppm), which arise from $^{13}C$ and $^{34}S$.[21] By applying a reduction potential of −2 V across the working electrode, the abundances of $m/z$ 307.0844, 307.5858, and 308.0821 decreased, which was ascribed to the consumption of GSSG during electrolytic reaction. We also found a new peak at $m/z$ 308.0921 (theoretical $m/z$ 308.0911, error +3.2 ppm), which was assigned to the protonated GSH cation $[GSH + H]^+$. EICs at $m/z$ 307.0844, 307.5855, and 308.0838 in Figure 4b demonstrated the correlation of their decrease with the application of the reduction potential.

We then switched the MS operation mode from positive to negative. The spectra were collected by individually applying a 0 to −2 V potential. A comparison between both spectra (Figure 4c) indicated the formation of a new peak at 306.0741 (theoretical $m/z$ 306.0765, error −7.8 ppm), which corresponded to the deprotonated GSH anion $[GSH - H]^-$. Similar dependence of the peak at 306.0741 on the application of the reduction potential was also obtained (Figure 4d), which provided evidence for the disulfide breakdown of GSSG by electro-reduction.

**Observing the DMDPA Nitrenium Ion in an Electro-Oxidation Reaction.** Nitrenium ions are reactive intermediate species based on nitrogen with two substituents as well as both an electron lone pair and a positive charge. Involvement of nitrenium ions in numerous chemical reactions, including ones that damage DNA, motivates fundamental studies into their structures and behaviors.[25,26]

We used EC-DESI with the flat plane to probe arylamine nitrenium intermediates from electrochemical generation and demonstrate the feasibility of the device for online electrochemistry monitoring. Electrochemical oxidation of DMDPA (Scheme 2) is proposed to follow first loss of one electron from DMDPA (**6**) and to generate the radical cation intermediate $DMDPA^{\cdot+}$ (**7**) (theoretical $m/z$ 229.1097). This step then is


DOI: 10.1021/acs.analchem.6b05124
Anal. Chem. 2017, 89, 3191−3198

followed by losses of an electron and a proton to give rise to the DMDPA nitrenium ion (**8**) (theoretical *m/z* 228.1019).[27,28]

When 100 μM DMDPA solution in 1 mM LiOTf in acetonitrile was sprayed onto the surface of the wetted carbon paper at a flow rate of 5 μL $min^{-1}$, a cation peak of *m/z* 230.1175 was observed in the mass spectrum (Figure 5a), which was ascribed to protonated DMDPA (**5**) (theoretical *m/z* 230.1176, error −0.4 ppm). Also observable was a peak of *m/z* 229.1098, corresponding to the $DMDPA^{\bullet+}$ (**7**) (error +0.4 ppm). After the application of a 5 V potential, the mass spectrum (Figure 5a) showed a new peak of *m/z* 228.1020, which is the contribution from the DMDPA nitrenium ion (**8**) (error +0.4 ppm). Besides, the mass spectrum (Figure 5a) also showed the decreased abundance of *m/z* 230.1175 (**5**) but the increased abundance of *m/z* 229.1098 (**7**), indicating the consumption of DMDPA (**6**) and the production of $DMDPA^{\bullet+}$ (**7**) during electrolysis. Upon CID (see the Supporting Information Figure S7), the DMDPA nitrenium ion (**8**) gave rise to fragment ions of *m/z* 213.0783 (theoretical *m/z* 213.0784, error −0.5 ppm) and 197.0834 (theoretical *m/z* 197.0835, error −0.5 ppm) by the losses of a methyl and a methoxy, respectively, confirming its structure. Consecutive applications of 0 V, 5 V, and 0 V potentials across the working electrode yielded a low stable signal line at the start and at the end with sharp peak profiles at *m/z* 229.1098 (**7**) and 228.1020 (**8**) (Figure 5b). The same phenomena were observed in two replicate measurements. These results proved the dependence of the DMDPA radical cation (**7**) and the DMDPA nitrenium ion (**8**) on the applied oxidation potential as a result of electrochemical oxidation. The results were in line with previous work.[15]

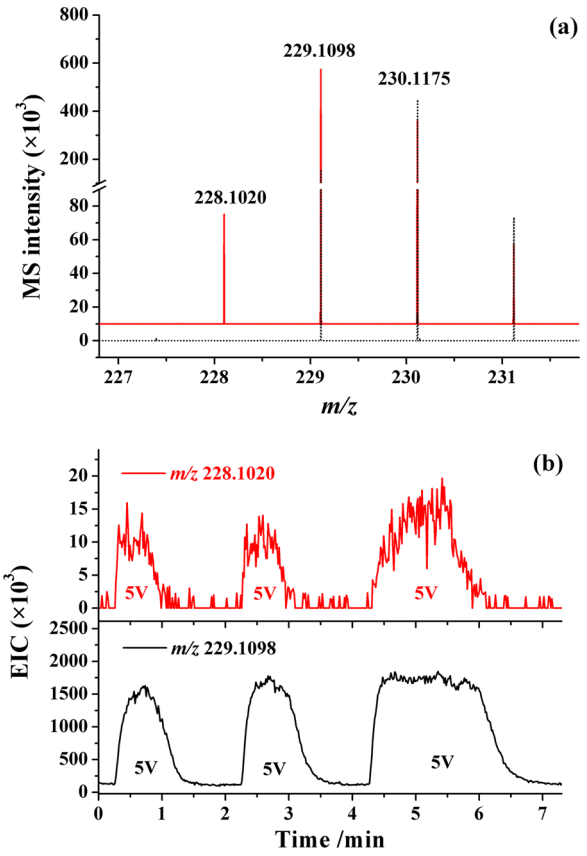


**Figure 5.** (a) Positive-ion-mode mass spectra of DMDPA with 0 (gray) and 5 V (red) applied to the carbon paper. (b) Ion chronograms showing extracted ion counts for the DMDPA nitrenium ion at *m/z* 228.1020 (red) and the DMDPA radical cation at *m/z* 229.1098 (black) as the potential is turned on and off.

**Monitoring DPTA Nitrenium Ion in Electro-Oxidation.** Electrochemical oxidation of DPTA (Scheme 3) follows similar electro-oxidation pathways to that of DMDPA. There is an initial loss of one electron from DPTA (**10**) to give rise to the radical cation intermediate $DPTA^{\bullet+}$ (**11**) (theoretical *m/z* 197.1199), and further losses of an electron and a proton to produce the DPTA nitrenium ion (**12**) (theoretical *m/z* 196.1121).[15]

When 5 μL $min^{-1}$ of 100 μM DPTA solution in 1 mM LiOTf in acetonitrile was sprayed onto the carbon paper, the mass spectrum (Figure S8a) showed a major peak at *m/z* 198.1273, ascribed to the protonated DPTA cation $[DPTA + H]^+$ (**9**) (theoretical *m/z* 198.1277, error −2.0 ppm), and a minor peak at *m/z* 197.1196, arising from the radical cation intermediate $DPTA^{\bullet+}$ (**11**) (error −1.5 ppm). When an oxidation potential of 5 V was applied across the carbon paper, a new peak at *m/z* 196.1118, corresponding to the DPTA nitrenium ion (**12**) (error −1.5 ppm), and the enhanced abundance at *m/z* 197.1196 (**11**) were observed (Figure S8a). By using CID (see the Supporting Information Figure S9), the DPTA nitrenium ion (**12**) lost a methyl, leading to the formation of the fragment ion at *m/z* 181.0881 (theoretical *m/z* 181.0886, error −2.8 ppm).[15] When consecutive applications of the 0 V and 5 V potentials across the working electrode were tried three times, three peaks were observed by ion extraction at *m/z* 196.1118 (**12**) and 197.1196 (**11**) (Figure S8b). These observations confirmed that these species stemmed from the electrochemical oxidation of DPTA.

## CONCLUSIONS

Two simple, robust, and reliable EC-DESI-MS devices capable of probing of transient intermediates in electrochemical reactions were presented. Both were achieved by the introduction of porous conducting carbon paper as the working electrode in the forms of either a grooved inclined plane or a flat front-surfaced plane. Radical cation intermediates from electro-dimerization of TPA and transient diimine species from the electro-oxidation of uric acid were successfully captured from the grooved inclined carbon tape. Electrochemical cleavage of disulfide bond from glutathione was also accomplished by the same instrumentation. Fleeting nitrenium

**Scheme 3. Oxidation Steps and Ion Formation Pathways of DPTA**

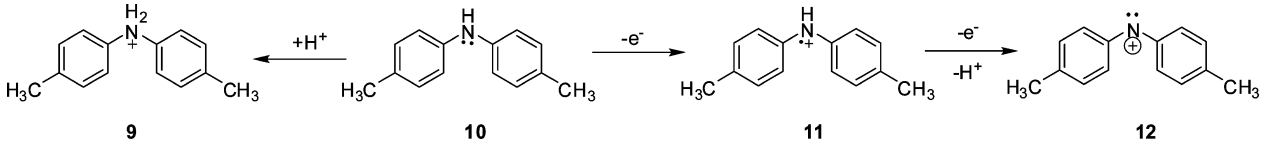




DOI: 10.1021/acs.analchem.6b05124
Anal. Chem. 2017, 89, 3191−3198

ions generated in the electro-oxidation of DMDPA and DPTA were successfully captured from the flat-front-surfaced carbon tape. The flat porous carbon tape surface might be advantageous over the inclined plane because of its ease of setup. By taking advantage of high sensitivity, selectivity, and accuracy of MS detection with collision induced dissolution, we find that EC-DESI-MS is a powerful analytical tool to elucidate mechanistic information on many electrochemical redox reactions.

## ■ ASSOCIATED CONTENT

### Supporting Information

The Supporting Information is available free of charge on the ACS Publications website at DOI: 10.1021/acs.analchem.6b05124.

Text, mass spectra, figures giving experimental details, optimization of experimental conditions, and applications of the two devices in studying electro-oxidation behaviors (PDF)

Video showing weak whirling flows in the water-filled culture dish using the custom DESI sprayer incorporated with the gas shield with the 0.35-mm-diameter hole for microdroplets passage at a $N_2$ pressure of 150 psi (MOV)

Video showing no visible water whirlpool in the water-filled culture dish using the custom DESI sprayer incorporated with the gas shield with the 0.35-mm-diameter hole for microdroplets passage at a $N_2$ pressure of 150 psi (MOV)

Video showing a turbulent water vortex in the water-filled culture dish using the custom DESI sprayer without a gas shield at a $N_2$ pressure of 120 psi (MOV)

## ■ AUTHOR INFORMATION


### Corresponding Author

*Phone: +1-650-723-3062. E-mail: zare@stanford.edu.

### ORCID

Richard N. Zare: 0000-0001-5266-4253


### Notes

The authors declare no competing financial interest.

## ■ ACKNOWLEDGMENTS

Heyong Cheng appreciates the financial support from the China Scholarship Council (Grant 201508330736) and the National Natural Science Foundation of China under Project No. 21405030. This work was also supported by the U.S. Air Force Office of Scientific Research under Project No. AFOSR FA9550-16-1-0113.

## ■ REFERENCES


(1) Faber, H.; Vogel, M.; Karst, U. *Anal. Chim. Acta* **2014**, *834*, 9−21.
(2) Oberacher, H.; Pitterl, F.; Erb, R.; Plattner, S. *Mass Spectrom. Rev.* **2015**, *34*, 64−92.
(3) Brown, J. H. *J. Chem. Educ.* **2016**, *93*, 1326−1329.
(4) Kaim, W.; Fiedler, J. *Chem. Soc. Rev.* **2009**, *38*, 3373−3382.
(5) Tian, Z.-Q.; Ren, B. *Annu. Rev. Phys. Chem.* **2004**, *55*, 197−229.
(6) Liu, P.; Lu, M.; Zheng, Q.; Zhang, Y.; Dewald, H. D.; Chen, H. *Analyst* **2013**, *138*, 5519−5539.
(7) Bruckenstein, S.; Gadde, R. R. *J. Am. Chem. Soc.* **1971**, *93*, 793−794.
(8) Volk, K. J.; Yost, R. A.; Brajter-Toth, A. *Anal. Chem.* **1992**, *64*, 21A−26A.
(9) Hambitzer, G.; Heitbaum, J. *Anal. Chem.* **1986**, *58*, 1067−1070.
(10) Volk, K. J.; Yost, R. A.; Brajter-Toth, A. *Anal. Chem.* **1989**, *61*, 1709−1717.
(11) Bartmess, J. E.; Phillips, L. R. *Anal. Chem.* **1987**, *59*, 2012−2014.
(12) Bökman, C. F.; Zettersten, C.; Nyholm, L. *Anal. Chem.* **2004**, *76*, 2017−2024.
(13) Xu, X.; Lu, W.; Cole, R. B. *Anal. Chem.* **1996**, *68*, 4244−4253.
(14) Zettersten, C.; Co, M.; Wende, S.; Turner, C.; Nyholm, L.; Sjöberg, P. J. R. *Anal. Chem.* **2009**, *81*, 8968−8977.
(15) Brown, T. A.; Hosseini-Nassab, N.; Chen, H.; Zare, R. N. *Chem. Sci.* **2016**, *7*, 329−332.
(16) Brown, T. A.; Chen, H.; Zare, R. N. *J. Am. Chem. Soc.* **2015**, *137*, 7274−7277.
(17) Brown, T. A.; Chen, H.; Zare, R. N. *Angew. Chem., Int. Ed.* **2015**, *54*, 11183−11185.
(18) Brownell, K. R.; McCrory, C. C. L.; Chidsey, C. E. D.; Perry, R. H.; Zare, R. N.; Waymouth, R. M. *J. Am. Chem. Soc.* **2013**, *135*, 14299−14305.
(19) Miao, Z.; Chen, H. *J. Am. Soc. Mass Spectrom.* **2009**, *20*, 10−19.
(20) Zheng, Q.; Chen, H. *Annu. Rev. Anal. Chem.* **2016**, *9*, 411−448.
(21) Li, J.; Dewald, H. D.; Chen, H. *Anal. Chem.* **2009**, *81*, 9716−9722.
(22) Liu, P.; Lanekoff, I. T.; Laskin, J.; Dewald, H. D.; Chen, H. *Anal. Chem.* **2012**, *84*, 5737−5743.
(23) Abd-El-Latif, A. A.; Bondue, C. J.; Ernst, S.; Hegemann, M.; Kaul, J. K.; Khodayari, M.; Mostafa, E.; Stefanova, A.; Baltruschat, H. *TrAC, Trends Anal. Chem.* **2015**, *70*, 4−13.
(24) Perry, R. H.; Splendore, M.; Chien, A.; Davis, N. K.; Zare, R. N. *Angew. Chem., Int. Ed.* **2011**, *50*, 250−254.
(25) Falvey, D. E. In *Reactive Intermediate Chemistry*; John Wiley & Sons, Inc., 2005; pp 593−650.
(26) Gassman, P. G. *Acc. Chem. Res.* **1970**, *3*, 26−33.
(27) Serve, D. *J. Am. Chem. Soc.* **1975**, *97*, 432−434.
(28) Svanholm, U.; Parker, V. D. *J. Am. Chem. Soc.* **1974**, *96*, 1234−1236.




DOI: 10.1021/acs.analchem.6b05124
*Anal. Chem.* 2017, 89, 3191−3198